SUPPLEMENTARY FIGURE LEGENDS

Sup. Fig. S1. Kinetics of PARP-1 WT and Zn3 mutants automodification performed using a colorimetric assay. Time points in the linear portion of the reaction profile were measured for several NAD^+ concentrations to provide initial rates in pmol of ADP-ribose/s. Initial rates were plotted versus total NAD^+ concentration and fitted using the Michaelis-Menton model to the data and yielded K_M (μM) and V_{MAX} (pmol/s). *A*. Example of a Michaelis-Menton plot of a DNA-dependent experiment for WT, W318R, and T316A mutant. The reactions were performed in the presence of 20 nM protein and 40 nM DNA. *B*. Example of a Michaelis-Menton plot of a DNA-independent experiment for WT, W318R and T316A mutant. The reactions were performed in the presence of 60 nM protein.

Sup. Fig. S2. Binding affinity of PARP-1 WT and Zn3 mutants. The binding affinity was determined by fluorescence polarization using an 18-basepair (bp) duplex containing a fluorescein derivative (6-FAM). The reactions were performed with 5 nM of probe and various concentrations of protein. The observed binding constant was obtained from a non-linear least squares fit to the data using a two state binding model.

Sup. Fig. S3. Analytical gel filtration elution profiles for full-length WT PARP-1 and W318R PARP-1. 50 μL of WT PARP-1 (43 μM) or W318R (100 μM) were injected onto a 24 mL analytical S200 Superdex column (GE Healthcare). Proteins were eluted with isocratic flow of 40 mL of buffer (20 mM Hepes pH 8.0, 150 mM NaCl, 0.1 mM TCEP, 1 mM EDTA). 0.5 ml fractions were collected and absorbance at 280 nm was recorded. This column has an 8 mL void volume. The two PARP-1 proteins elute at the same volume with the same peak shape. The difference in peak height is proportional to the difference in protein concentration loaded.

Sup. Fig. S4. CD spectra for full-length WT PARP-1 and W318R PARP-1. CD wavelength scans (280–200 nm) were performed at 4 °C in a quartz cuvette of 1 mm path length on a JASCO J-810 spectropolarimeter. The protein was at 2.5 μM in a buffer composed of 5 mM Na,KPO_4, pH 7.5, 50 mM Na_2SO_4, and 0.1 mM TCEP. Each spectrum represents the average of three scans. The two PARP-1 proteins have similar spectra, indicating that there are no major structural differences between the two proteins.

Sup. Fig. S5. Mutations at the Zn3 dimer interface do not disrupt PARP-1 DNA-dependent activity. *A*. Zn3 crystallographic dimer with mutated residues shown in blue and numbered. A key for the numbering

is shown in panel C. *B*. The monomeric NMR structure with mutated residues as shown in A. Amino acid P359 (#10) was not present in the Zn3 domain construct used in the NMR study, and is therefore not shown in panel B. *C*. DNA-dependent activity of WT PARP-1 and Zn3 dimer mutants (0.62 mM) with 1 μM duplex DNA and 5 mM NAD^+.

Supplementary Figure S1

A

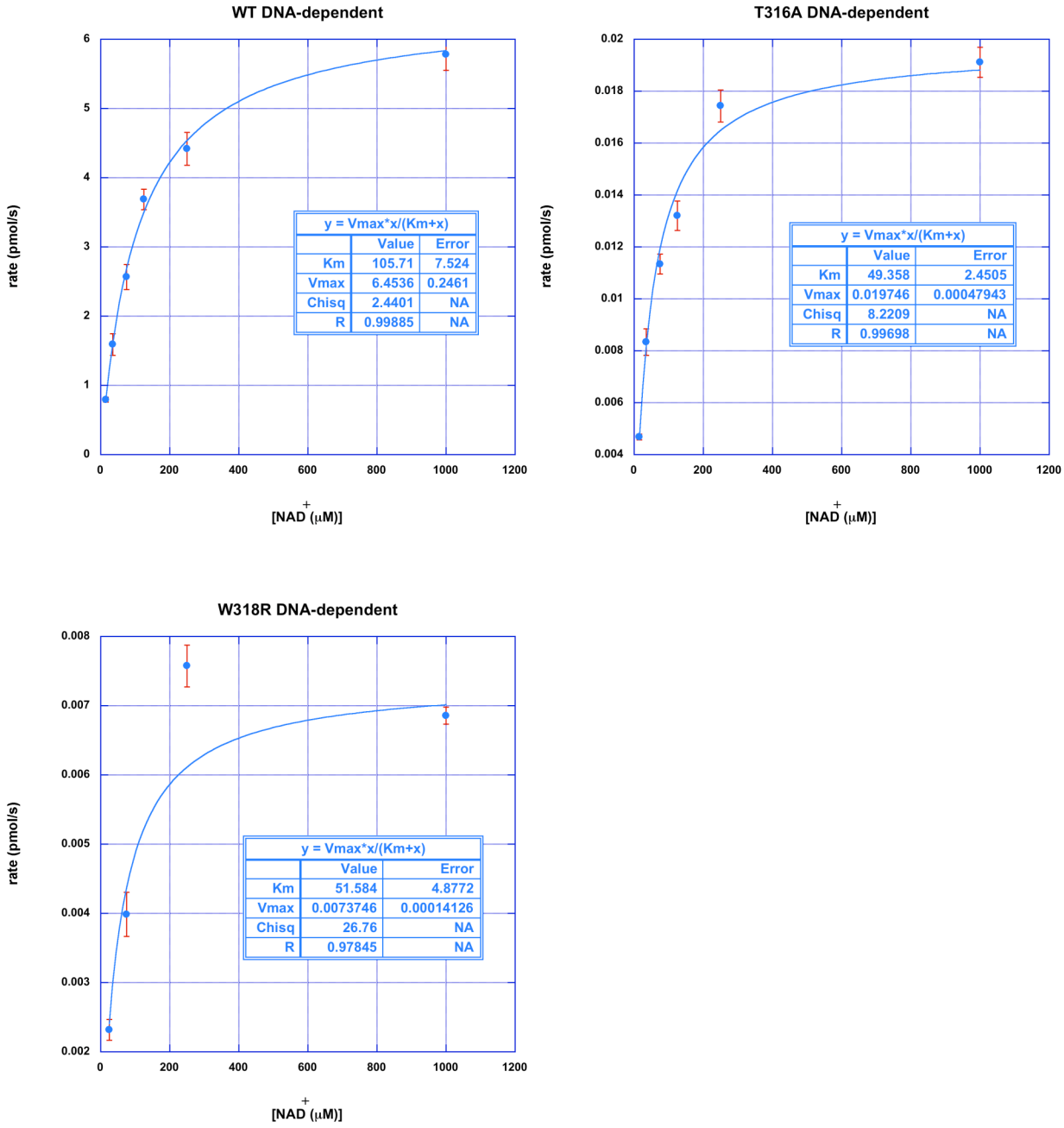

Supplementary Figure S1

B

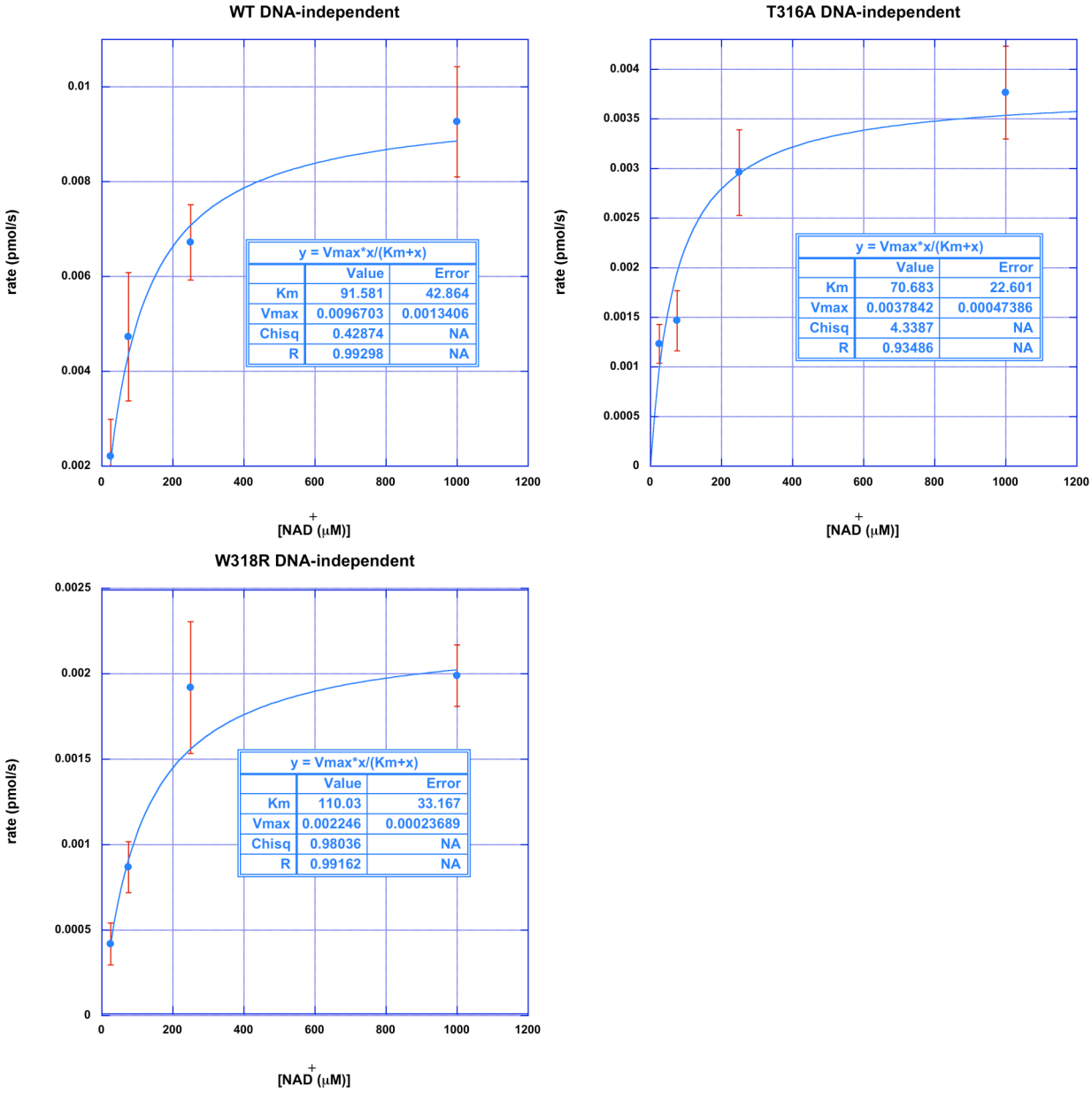

Supplementary Figure S2

Zn ribbon mutants

	K_D	error ±
WT	14.42	2.2
D314A	20.86	2.76
V315A	12.21	2.25
T316A	23.14	4.36
T316S	13.53	1.68
A317G	14.74	3.88
A317S	20.15	4.89
W318R	19.53	1.63
W318F	16.77	1.69
W318A	25.02	2.89
T319A	14.07	1.55
K320A	5.04	1.07

Dimer interface mutants

	K_D	error ±
WT	12.61	2.16
Q241L	15.25	1.89
R340E	12.61	1.68
E341R	9.57	1.18
Y344D	12.03	2.46
L345D	15.79	1.39
R355D	29.46	2.76
F357D	22.77	2.04
F357Y	10.77	2.5
L348D/V350D	12.18	1.69
P358G/P359G	not determined	

Supplementary Figure S3

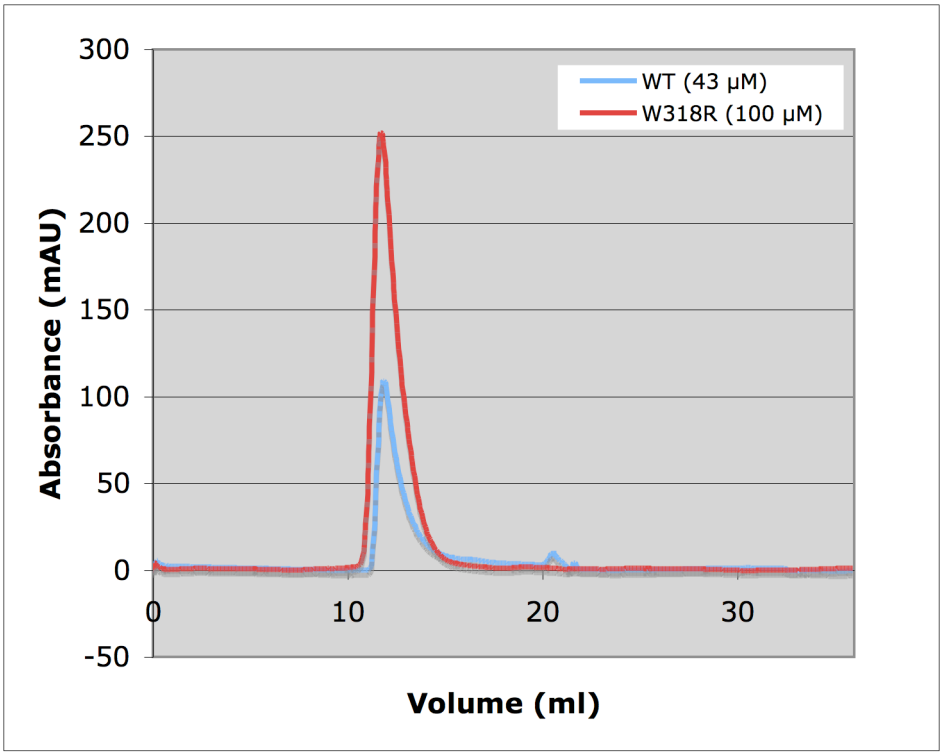

Supplementary Figure S4

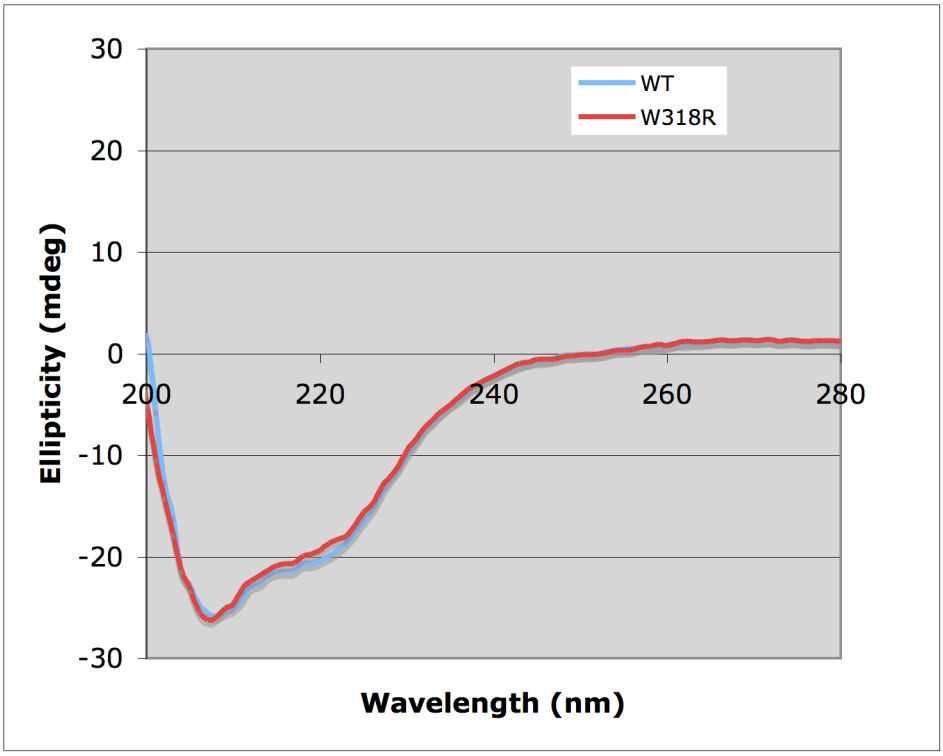

Supplementary Figure S5